

Article

Influence of the $\text{LaMn}_{1-x}\text{Fe}_x\text{O}_3$ ($x = 0-1$) Composition on Catalytic Activities in the Reactions Involving Oxygen

Lyubov Isupova ^{*}, Vladimir Rogov, Evgenii Gerasimov  and Igor Prosvirin

Boreskov Institute of Catalysis SB RAS, 630090 Novosibirsk, Russia

^{*} Correspondence: isupova@catalysis.ru; Tel.: +7-(383)-3269603

Abstract: Perovskite samples of the $\text{LaMn}_{1-x}\text{Fe}_x\text{O}_3$ ($x = 0-1$) series were prepared by the Pechini method; their physicochemical properties were studied using XRD, HRTEM, XPS, and BET, and their catalytic activity was estimated in nitrous oxide decomposition and methane and CO oxidation reactions. In methane and CO oxidation reactions, all intermediate ($0 < x < 1$) samples of the series exhibited a lower catalytic activity normalized to the unit surface area as compared to the extreme terms, whereas in the nitrous oxide decomposition all intermediate samples were more active than extreme terms of the series. Different dependences of activities on the composition obtained in the study for the tested reactions involving the catalyst oxygen are caused by differences in the reaction mechanisms.

Keywords: perovskites; methane oxidation; N_2O decomposition; weakly bound oxygen



Citation: Isupova, L.; Rogov, V.; Gerasimov, E.; Prosvirin, I. Influence of the $\text{LaMn}_{1-x}\text{Fe}_x\text{O}_3$ ($x = 0-1$) Composition on Catalytic Activities in the Reactions Involving Oxygen. *Catalysts* **2022**, *12*, 1563. <https://doi.org/10.3390/catal12121563>

Academic Editors:
Alexander Kokorin and Detlef
W. Bahnemann

Received: 10 October 2022
Accepted: 30 November 2022
Published: 2 December 2022

Publisher's Note: MDPI stays neutral with regard to jurisdictional claims in published maps and institutional affiliations.



Copyright: © 2022 by the authors. Licensee MDPI, Basel, Switzerland. This article is an open access article distributed under the terms and conditions of the Creative Commons Attribution (CC BY) license (<https://creativecommons.org/licenses/by/4.0/>).

1. Introduction

Owing to the high thermal and chemical stability as well as the unique catalytic, electrophysical and magnetic properties of oxides with the LaBO_3 perovskite structure, they are considered as promising materials for some high-temperature processes; for example, such oxides can be used as the high-temperature cathode or anode materials for solid oxide fuel cells, as the catalysts for oxidative conversion of methane and combustion of waste gases, particularly the exhaust gases from motor vehicles, and as the catalysts for high-temperature oxidation of ammonia and decomposition of nitrous oxide in the production of nitric acid [1–5]. The perovskites containing Mn or Fe cations in the B sublattice are considered to be among the most active and stable ones in the catalytic processes involving oxygen [3,4]. Since the activity of the oxide catalysts in such high-temperature catalytic processes depends mostly on the oxygen bond strength on the surface, their activity is often controlled by the introduction of substituting cations with different valences into lanthanum sublattice. Their introduction affects the defective structure of the oxide or its structural modification, thus changing the oxygen amount or leading to the appearance of new oxygen species [6–9]. In addition, the activity of perovskites is also affected by the method of their preparation [8,10–12].

Lanthanum manganite and lanthanum ferrite have different defect structures. Lanthanum manganite belongs to the oxides with excess oxygen; typically, it contains manganese cations in an increased oxidation state (+4) [13]. Lanthanum ferrite, on the contrary, is characterized by the presence of oxygen vacancies and a deficit of lanthanum in the lanthanum positions [14]. Thus, it is expected that the substitution of manganese cations by iron cations in position B will also affect the oxide defectiveness and the oxygen bond strength in the mixed perovskite, and hence the catalytic activity. Indeed, the literature data testify to such an effect, but it was different in different reactions.

It was thus demonstrated in [10] that the catalytic activity in CO oxidation (the conversion degree of CO) of the $\text{LaMn}_{1-x}\text{Fe}_x\text{O}_3$ ($0 < x < 1$) perovskites prepared by the precipitation or citrate method and calcined at 800 °C changed through a maximum at

$x = 0.6$ due to the highest specific surface area of the sample, while the activity normalized per m^2 was higher for LaMnO_3 ($x = 0$). It was noted that the introduction of iron increased the $\text{Mn}^{3+}/\text{Mn}^{4+}$ ratio and decreased the unit cell parameter of the perovskite structure from 3.931 \AA for lanthanum manganite to 3.8743 \AA for lanthanum ferrite. The influence of the $\text{LaMn}_{1-x}\text{Fe}_x\text{O}_3$ ($0 < x < 1$) preparation method on the activity was also revealed: the samples prepared by the citrate method were more active.

A recent study undertaken by Miao et al. [8] revealed the high catalytic activity of the $\text{La}(\text{Mn, Fe})\text{O}_{3+\lambda}$ catalyst in low and middle temperature methane oxidation and the effects of different preparation conditions on the catalyst (the composition was not given) performance. The results showed that the single-phase perovskite $\text{La}(\text{Mn, Fe})\text{O}_{3+\lambda}$ catalyst stable in methane oxidation could be prepared by the sol-gel method after calcination at $600 \text{ }^\circ\text{C}$ for 3 h in the air atmosphere. The highest activity in methane combustion in the middle and low temperature regions was revealed for the $\text{La}(\text{Mn, Fe})\text{O}_{3+\lambda}$ catalyst when ethylene glycol/metals ratio = $1/2$ and citric acid/metals ratio = $1/2$ were obtained after its calcination at $600 \text{ }^\circ\text{C}$. The catalyst had a high specific surface area ($29.2 \text{ m}^2/\text{g}$), pore volume ($0.19 \text{ cm}^3/\text{g}$), pore diameter (27.8 nm), and a higher $\text{Mn}^{3+}/\text{Mn}^{4+}$ ratio on the surface.

In [15], single-phase perovskites $\text{LaMn}_{1-x}\text{Fe}_x\text{O}_3$ ($0 < x < 1$) were prepared by the sol-gel method, calcined at $700 \text{ }^\circ\text{C}$, and studied in the $\text{NO} + \text{CO}$ catalytic reduction over the temperature region of $150\text{--}500 \text{ }^\circ\text{C}$. It was shown that the introduction of iron, on the contrary, decreases the specific surface area of the samples, increases the fraction of Me^{4+} cations on the surface, and facilitates the reduction of perovskites. Thus, the maximum activity (the conversion of CO and NO) in this reaction at $350 \text{ }^\circ\text{C}$ was observed for a sample with the composition $\text{LaMn}_{0.3}\text{Fe}_{0.7}\text{O}_3$ and low specific surface area.

In [16], single-phase perovskites $\text{LaMn}_{1-x}\text{Fe}_x\text{O}_3$ ($0 < x < 1$) were prepared by the method of polymer-salt compositions (Pechini) after thermal treatment of polymer-salt precursors at $800 \text{ }^\circ\text{C}$. The authors of [16] revealed an increase in the lattice parameter of the perovskite (in a cubic approximation) from 3.885 to 3.944 \AA with raising the iron content (in contrast to [10]), the specific surface area of the samples showed slight changes in the range of $11\text{--}15 \text{ m}^2/\text{g}$. The TPR data indicate a higher reducibility of manganese cations and, on the contrary, an increase in stability of iron cations in the obtained mixed perovskites; the catalytic activity in hydrogen peroxide decomposition decreased with raising the iron content in the x series: $0 \sim 0.27 \gg 0.57 \gg 0.90$. A high activity of $\text{LaMn}_{1-x}\text{Fe}_x\text{O}_3$ ($0 < x < 0.15$) perovskites in the soot oxidation reactions was demonstrated in [17].

The authors of [18] investigated the electronic, structural and magnetic properties of the $\text{LaMn}_{1-x}\text{Fe}_x\text{O}_3$ ($0 < x < 1$) perovskites obtained by the glycine-nitrate synthesis and calcined at $1000 \text{ }^\circ\text{C}$ in air. It was found that the samples with $x < 0.5$, similar to $\text{LaMnO}_{3+\delta}$, are the rhombohedral perovskites containing excess oxygen, whereas the samples with $x \geq 0.5$ are the orthorhombic perovskites not containing excess oxygen, which are antiferromagnets with the predominant exchange interaction Fe-O-Fe .

Data reported in the literature indicate that a continuous series of single-phase solutions can appear in the $\text{LaMn}_{1-x}\text{Fe}_x\text{O}_3$ ($0 < x < 1$) system already after thermal treatment at $600 \text{ }^\circ\text{C}$, which is promoted by a homogeneous distribution of cations at the stage of precursor synthesis (Pechini, citrate and sol-gel methods). The literature data also indicate that the morphotropic phase transition occurs in the system in the region of $x = 0.5$. The high catalytic activity of $\text{LaMn}_{1-x}\text{Fe}_x\text{O}_3$ perovskites in some reactions was revealed, but the regularities describing changes in the catalytic activity of oxides with an increase in the content of iron cations are contradictory; this may be related to different methods of sample preparation in the studied catalytic reactions or to the different action of reaction media on the catalysts, which may change the chemistry of catalysts. For example, the authors of [19], when studying the $\text{La}_{1-x}\text{Ca}_x\text{MnO}_3$ samples prepared by the Pechini method before and after testing in methane oxidation, observed the appearance of structurally ordered regions on the surface after testing and an increase in the calcium content, which led to a decrease in their activity.

The $\text{LaMn}_{1-x}\text{Fe}_x\text{O}_3$ perovskites may be of interest not only as the catalysts for deep oxidation processes, but also as the catalysts for high-temperature N_2O decomposition because the substitution of manganese cations by iron cations in position B will affect the oxygen bond strength and the catalytic activity in N_2O decomposition as well as taking into account the reaction limiting stage (oxygen desorption) according to [3]. Thus, in the N_2O decomposition there is no possible influence of CO_2 on the catalyst activity as compared with methane and CO oxidation.

To elucidate a possible role of the reaction medium, three different catalytic processes occurring with the involvement of the catalyst oxygen were chosen for the investigation of oxides prepared by the Pechini method. The oxidation of methane, which is the most difficult to oxidize among hydrocarbons, and the high-temperature nitrous oxide decomposition are catalytic processes of practical interest. It is also reasonable to estimate the activity of oxides in CO oxidation, which will allow us to compare experimental and literature data for revealing the role of the preparation method.

The Pechini method implies the absence of liquid effluents and is often used for catalyst preparation because it allows the synthesis of mixed single-phase oxides at moderate calcination temperatures and provides a more uniform distribution of oxides on the support surface during the synthesis of supported catalysts.

The goal of the study was to investigate the catalytic properties of $\text{LaMn}_{1-x}\text{Fe}_x\text{O}_3$ ($0 < x < 1$) perovskites prepared by the Pechini method in different catalytic reactions that proceed with the involvement of the catalyst oxygen—nitrous oxide decomposition, oxidation of methane and CO—in order to assess the contributions of reaction medium and preparation method to the regularities describing changes in the catalytic activity of the oxides with variation of x .

2. Results and Discussion

2.1. Catalysts Characterization

As shown by XRD analysis (Figure 1a and Table 1), all the samples of the $\text{LaMn}_{1-x}\text{Fe}_x\text{O}_3$ series are well crystallized (the SCR size of ca. 66–95 nm) single-phase solid solutions with the perovskite structure.

The unit cell parameters of oxides listed in Table 1 indicate that the unit cell volume of the solid solution increases with the iron content (Figure 1b), which is consistent with the data reported in [16]. Taking the close ionic radii of Fe^{3+} and Mn^{3+} cations into account, it can be assumed that the observed growth of the lattice parameter is caused by an increase in the number of oxygen vacancies in the structure of perovskites that occurs with the increase in iron content. The formation of vacancies may be promoted by the reducing conditions that are implemented during the preparation of oxides by the Pechini method, in contrast to the data of [10].

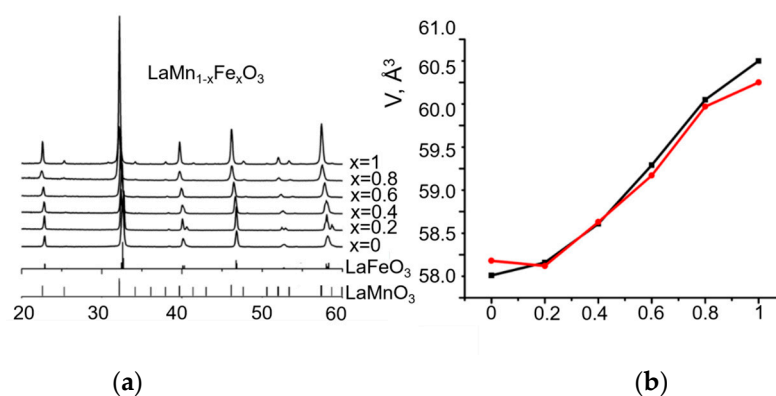


Figure 1. X-ray diffraction patterns of $\text{LaMn}_{1-x}\text{Fe}_x\text{O}_3$ perovskites before catalytic testing (a) and the unit cell volume in dependence x before (—■—) and after (—●—) testing (b) in methane oxidation.

Table 1. X-ray diffraction analysis data for $\text{LaMn}_{1-x}\text{Fe}_x\text{O}_3$ perovskites before and after testing in methane oxidation.

Sample	Space Group	Unit Cell Parameters before Testing	Unit Cell Parameters after Testing	D (Å) before Testing	D (Å) after Testing	$\Delta d/d \cdot 10^4$ before Testing	$\Delta d/d \cdot 10^4$ after Testing	Ssp, m^2/g
LaMnO_3	Pnmb *	a = 5.491 (8) b = 7.774 (4) c = 5.489 (9)	a = b = 5.526 (3) c = 13.324 (8)	660	660	3.9	4.5	3.2
$\text{LaMn}_{0.8}\text{Fe}_{0.2}\text{O}_3$	R-3c	a = b = 5.514 (1) c = 13.310 (1)	a = b = 5.513 (1) c = 13.307 (1)		>1000	-	-	4.3
$\text{LaMn}_{0.6}\text{Fe}_{0.4}\text{O}_3$	R-3c	a = b = 5.521 (1) c = 13.352 (4)	a = b = 5.517 (1) c = 13.310 (2)	-	-	-	-	6.0
	Pnma	a = 5.486 (1) b = 7.769 (1) c = 5.524 (1)	a = 5.486 (1) b = 7.771 (1) c = 5.525 (1)	950	860	1.8	5.9	
$\text{LaMn}_{0.4}\text{Fe}_{0.6}\text{O}_3$	Pnma	a = 5.512 (1) b = 7.805 (1) c = 5.536 (1)	a = 5.502 (1) b = 7.812 (1) c = 5.530 (1)	920	920	7.4	11.0	8.4
$\text{LaMn}_{0.2}\text{Fe}_{0.8}\text{O}_3$	Pnma	a = 5.543 (1) b = 7.832 (1) c = 5.556 (1)	a = 5.540 (1) b = 7.829 (1) c = 5.554 (1)	750	650	11.0	10.0	10.0
LaFeO_3	Pnma	a = 5.563 (1) b = 7.860 (1) c = 5.560 (1)	a = 5.555 (2) b = 7.852 (2) c = 5.549 (1)	900	1000	10.0	20.0	6.1

* R3c/2 after testing.

It should be noted that in the synthesized series of samples, the morphotropic phase transition caused by an increase in the content of iron cations in oxides is observed in the composition range of $x \sim 0.4$. Samples with $x < 0.4$ are the rhombohedral perovskites, whereas samples with $x > 0.4$ are the orthorhombic ones. The $\text{LaMn}_{0.6}\text{Fe}_{0.4}\text{O}_3$ sample with $x = 0.4$ is characterized by the co-existence of two phases having the perovskite structure, the orthorhombic and rhombohedral ones. The analysis of micro-distortions calculated by the Williamson-Hall formula (Table 1) shows that their number in the oxide structures increases with the content of Fe cations, probably due to the growth in the number of oxygen vacancies in the oxide structure. The presence of the morphotropic phase transition at $x \sim 0.4$ revealed in this study, instead of $x = 0.5$, which was reported in [18], may be caused by the difference in the content of vacancies in the oxides prepared under different conditions (the Pechini method in this study and the glycine-nitrate method in [18]) or by possible deviations of the real stoichiometric ratio of cations in the oxides used in our study and in the cited work.

Although the phase composition of lanthanum manganite does not change after catalytic testing in methane oxidation (Table 1), a change in its structural modification and an increase in the unit cell volume are observed, which are typical of the polymorphous high-temperature transition [20], and may be caused by a decrease in the content of excess oxygen in the sample under the action of reaction medium. Noteworthy also is a decrease in the unit cell volumes against the background of the increased number of micro-distortions in the structure of iron-containing rhombohedral perovskites after testing (Table 1 and Figure 1b) and insignificant changes in the SCR size, which may testify to the association of point defects and the formation of extended ones. After testing, the $\text{LaMn}_{0.6}\text{Fe}_{0.4}\text{O}_3$ sample retains two modifications (orthorhombic and rhombohedral). Thus, the reaction medium of methane oxidation substantially increases the content of vacancies in oxides, facilitating the polymorphous transition in the case of lanthanum manganite or their ordering in the case of iron-containing perovskites.

The observed differences in the $\text{LaMn}_{1-x}\text{Fe}_x\text{O}_3$ oxides prepared by the Pechini method may affect their catalytic properties, which can lead to different changes in the activity of

such oxides in the reactions involving oxygen. Furthermore, it can be expected that an additional effect on the activity may be exerted by the reaction medium.

According to HRTEM data (Figure 2), the synthesized samples are also the single-phase solid solutions with the perovskite structure. The distinctive feature of this series of samples is the presence of pores on the surface, which formed upon removal of functional groups from the surface of the material. The perovskite particles have a rounded plate-like shape and a size of 100 nm–1 μm ; they merge into dendritic agglomerates with the size of several microns.

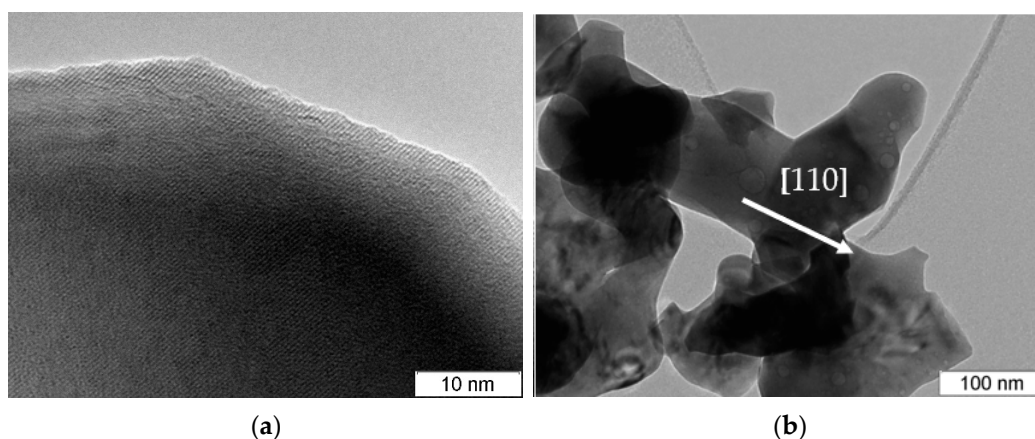


Figure 2. HRTEM images of the morphology (a) and crystal lattice (b) of the $\text{LaMn}_{0.8}\text{Fe}_{0.2}\text{O}_3$ sample.

After catalytic testing in methane oxidation, the samples also consist of the dendritic agglomerates comprising the rounded plate-like particles with a size from 100 nm to 1 μm . Pores with a widely varying size (from 1 to 100 nm) and amorphous carbon are observed on the surface of such well crystallized particles (Figure 3). Local orderings consisting in duplication of the unit cell period along (100) and (101) planes occur on some particles; this may be caused by the local ordering of Fe and Mn cations due to the Yan-Teller effect (Figure 4). The indicated local orderings are ca. 10 nm in size. Their formation may be related to the redistribution/ordering of Mn cations, which increases the number of micro-distortions in the oxide structure, primarily on the perovskite surface, because the corresponding reflections are not observed in the diffraction patterns. HRTEM did not detect any other visible changes in the structure or the presence of impurities except for those indicated above.

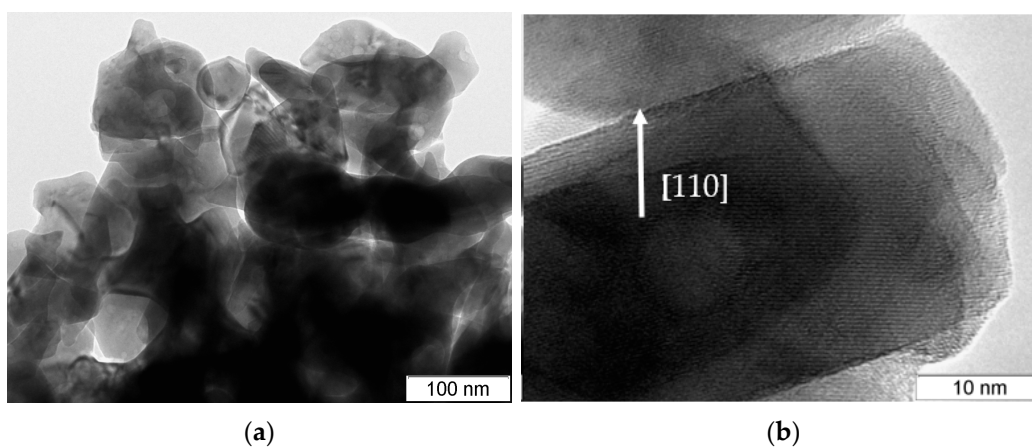


Figure 3. HRTEM images of morphology (a) and crystal lattice (b) of the $\text{LaMn}_{0.6}\text{Fe}_{0.4}\text{O}_3$ sample after methane oxidation.

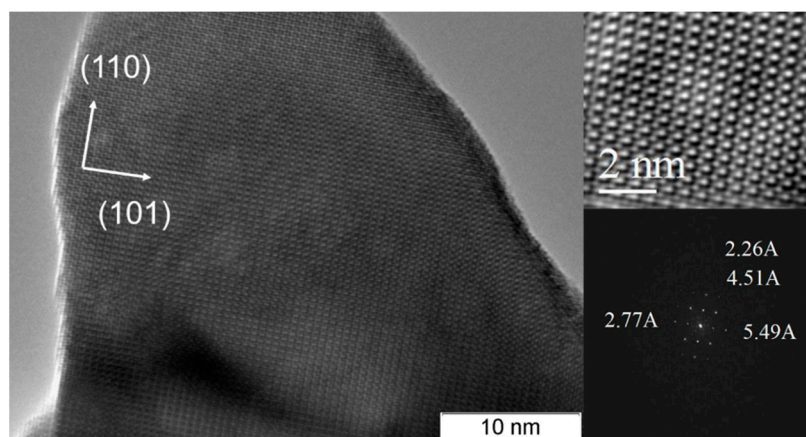


Figure 4. HRTEM image of the $\text{LaMn}_{0.2}\text{Fe}_{0.8}\text{O}_3$ microstructure after methane oxidation; FFT image illustrates duplication of the unit cell period along the (100) and (101) planes.

The data obtained allow for the conclusion that although the structure of oxides is stable in the reaction medium of methane oxidation, the content of oxygen vacancies in oxides increases under the action of reaction medium, which is accompanied by a decrease in the content of Mn^{4+} cations, the appearance of local regions with the ordered structure on the surface, and an increase in the number of micro-distortions. The appearance of carbon on the surface is also observed.

The data obtained allow for the conclusion that although the structure of oxides is stable in the reaction medium of methane oxidation, the content of oxygen vacancies in oxides increases under the action of the reaction medium, which is accompanied by a decrease in the content of Mn^{4+} cations, the appearance of local regions with the ordered structure on the surface, and an increase in the number of micro-distortions. The appearance of carbon on the surface is also observed.

XPS was used to investigate the surface composition of the series of $\text{LaMn}_{1-x}\text{Fe}_x\text{O}_3$ samples. The binding energies of $\text{Mn}2p_{3/2}$, $\text{Fe}2p_{3/2}$, $\text{La}3d_{5/2}$ and $\text{O}1s$ and relative concentrations (atomic ratios) of elements in the subsurface layer of catalysts, which were derived from XPS data, are listed in Table 2. According to XPS data for the tested catalysts, the surface of the samples is enriched with lanthanum cations because the atomic ratios $[\text{Fe}]/[\text{La}]$ and $[\text{Mn}]/[\text{La}]$ are lower than the stoichiometric ratio in the bulk of oxides. The $[\text{Fe}]/[\text{Mn}]$ atomic ratio is also lower than the stoichiometric one. As the iron content in the samples is raised, the content of manganese cations on the surface monotonically decreases, whereas the content of iron cations increases; however, their $([\text{Fe}]/[\text{Mn}])$ ratio is nearly two times lower than the stoichiometric value, which indicates that the surface of substituted perovskites is depleted with iron cations. In addition, with the increasing iron content in substituted samples, the fraction of lanthanum on the surface increases because the $[\text{Fe} + \text{Mn}]/[\text{La}]$ ratio decreases. Noteworthy also is a considerable growth of the carbon content on the surface of samples with the composition $x = 0.6$ and $x = 0.8$, which may testify to a higher content of residual carbon in the iron-containing perovskites.

According to XPS data, the lanthanum in the tested catalysts is in the La^{3+} state and enters the composition of perovskite and partially the composition of lanthanum carbonate $\text{La}_2(\text{CO}_3)_3$. Iron cations are present in the Fe^{3+} state in the octahedral environment of oxygen. Manganese cations in the catalysts under consideration are in the Mn^{3+} state. Since the binding energies of Mn^{3+} and Mn^{4+} cations are close, the presence of manganese cations in the Mn^{4+} state on the surface cannot be ruled out.

Table 2. Binding energies * of Mn2p_{3/2}, Fe2p_{3/2}, La3d_{5/2} and O1s (eV) and atomic ratios of elements in the subsurface layer of LaMn_{1-x}Fe_xO₃ oxides according to XPS data.

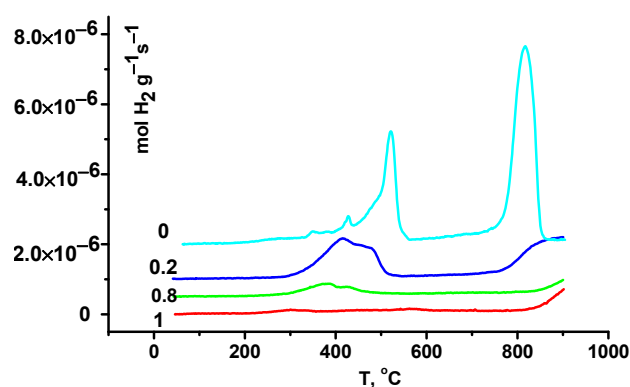
Oxide	Mn2p _{3/2}	Fe2p _{3/2}	La3d _{5/2}	O1s	[Fe]/[La]	[Mn]/[La]	[Fe]/[Mn]	[O]/[La]	[C]/[La]	[Fe+Mn]/[La]
LaMn _{0.8} Fe _{0.2} O ₃	642.29	710.95	834.26	529.51 531.27 533.33	0.06	0.51	0.13	3.11	1.53	0.57
LaMn _{0.6} Fe _{0.4} O ₃	642.30	710.91	834.29	529.57 531.56 533.62	0.14	0.39	0.35	2.92	1.33	0.53
LaMn _{0.4} Fe _{0.6} O ₃	642.31	710.85	834.48	529.96 532.15 533.92	0.17	0.28	0.62	3.14	3.13	0.45
LaMn _{0.2} Fe _{0.8} O ₃	642.35	710.79	834.37	529.85 532.07 533.75	0.23	0.15	1.51	3.20	3.12	0.38

* The binding energy scale was calibrated against the C1s line ($E_b = 284.80$ eV).

Thus, the substitution of manganese cations by iron leads to the depletion of the surface of substituted LaMn_{1-x}Fe_xO₃ oxides with 3d cations, which is more pronounced for iron cations, and to the enrichment of the surface with lanthanum cations, probably in the form of La₂(CO₃)₃.

As follows from the data of Table 1, the lowest specific surface area, 3.2 m²/g, is observed for unsubstituted samples of lanthanum manganite. The substitution of manganese cations by iron in the perovskite structure increases the specific surface area to 10 m²/g. The specific surface area of lanthanum ferrite is 6.1 m²/g. Thus, all of the substituted samples have a greater specific surface area than the unsubstituted ones.

Figure 5 and Table 3 present the H₂-TPR curves for LaMn_{1-x}Fe_xO₃ samples and the calculated amounts of hydrogen adsorbed by the samples. Two reduction regions are observed for the samples: at low and high temperatures. The adsorption in the low-temperature region (up to 550 °C) for LaMnO₃ and LaFeO₃ corresponds to the reduction of Mn⁴⁺ cations to Mn³⁺ or Fe³⁺ cations to Fe²⁺, respectively, whereas the adsorption in the high-temperature region—to the reduction of Mn³⁺ cations to Mn²⁺ or Fe²⁺ cations to Fe⁰.

**Figure 5.** H₂-TPR curves for LaMn_{1-x}Fe_xO₃ samples.

The introduction of iron at the retained structural modification of lanthanum manganite (the LaMn_{0.8}Fe_{0.2}O₃ sample) leads to a significant decrease in the reduction temperature that is virtually proportional to the manganese content decrease in the amount of adsorbed hydrogen in the first peak and, on the contrary, to an increase in the reduction temperature and a decrease in the adsorption in the second peak. This may indicate the promotion of the reduction of Mn⁴⁺ cations and, on the contrary, the hindering of the reduction of Mn³⁺ cations in this sample. A further increase in the content of iron cations significantly decreases the adsorption in the first and second peaks. Thus, the introduction of iron cations decreases the total adsorption (up to 900 °C) and adsorption in the low-temperature region (up to 550 °C), which is determined mostly by the reduction of Mn⁴⁺ cations; this is

accompanied by a considerable lowering of the temperature at which the reduction of the samples starts.

Table 3. Total (40–900 °C) and low-temperature (40–550 °C) hydrogen adsorption for $\text{LaMn}_{1-x}\text{Fe}_x\text{O}_3$ perovskites according to TPR data.

Sample	Adsorption in the Range of 40–900 °C, mol H ₂ /g	Adsorption in the Range of 40–550 °C, mol H ₂ /g	Temperature of Adsorption Maxima in the Range of 40–550 °C
LaMnO ₃	34.4×10^{-4}	13.1×10^{-4}	520
LaMn _{0.8} Fe _{0.2} O ₃	18.3×10^{-4}	9.64×10^{-4}	413
LaMn _{0.2} Fe _{0.8} O ₃	6.71×10^{-4}	3.58×10^{-4}	382
LaFeO ₃	5.8×10^{-4}	2.2×10^{-4}	300

2.2. Catalytic Activity in Methane and CO Oxidation and Nitrous Oxide Decomposition

Figure 6a displays the temperature dependence of methane conversion for $\text{LaMn}_{1-x}\text{Fe}_x\text{O}_3$ samples. As the testing temperature is raised, methane conversion increases, and complete conversion is achieved for all the samples already at 600 °C. The oxidation products are CO₂ and H₂O only. The highest conversion of methane at all the testing temperatures was observed for the lanthanum ferrite sample with $x = 1$ and for the mixed perovskite with the substitution degree $x = 0.4$ (the sample from the region of morphotropic phase transition). The observed dependence of activity of the samples on the composition in methane oxidation (Figure 6a) differs from the dependence reported in the literature [10], which was obtained in CO oxidation, probably due to the difference in the specific surface area of the samples. However, the data obtained testify that the conversion is determined not only by the specific surface area of samples because the sample with the highest specific surface area ($x = 0.8$) is not the most active one.

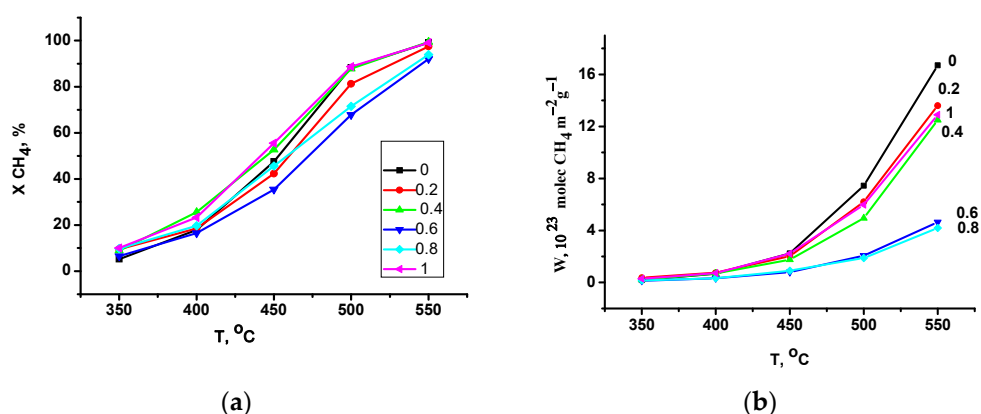


Figure 6. Temperature dependence of methane conversion (a) and methane oxidation rate (b) for $\text{LaMn}_{1-x}\text{Fe}_x\text{O}_3$ perovskites.

Indeed, normalization of the catalyst activity to the unit surface area (determination of the methane oxidation rate, Figure 6b) demonstrated that all the intermediate compositions were less active than the extreme terms of the series. Note that an increase in the x value decreased the normalized catalytic activity ($x = 0 > x = 0.2 \sim x = 0.4 \sim x = 1 \gg 0.6 \sim x = 0.8$); the lowest activity was observed for the samples with the composition $x = 0.6$ and 0.8 . In addition, it was shown that the activity of these samples additionally decreased upon testing. Thus, although methane conversion for the samples with $x = 0$, $x = 0.2$ and $x = 1$ does not change at 500 °C, its estimation after testing at 600 °C shows a significant decrease for the samples with $x = 0.6$ and 0.8 (by 8 and 13%, respectively). This may be caused by the imperfection of oxides and the surface properties related to the preparation method (Pechini

in this work), as well as by the features of the methane oxidation process, particularly the action of reaction medium on the catalyst.

Figure 7 shows CO conversion and the rate constant versus the testing temperatures. The dependence of normalized activity (k) on the composition in CO oxidation obtained in our study is nearly the same as the dependence obtained for methane oxidation, but differs from that reported in the literature for the samples prepared by the precipitation or citrate method [10]. The most active samples were those with $x = 0$ and $x = 1$. All the intermediate samples, as in the case of methane oxidation, exhibit a lower activity as compared to the extreme terms of the series ($x = 0 > x = 1 > x = 0.2 \sim x = 0.4 \sim x = 0.6 \sim x = 0.8$).

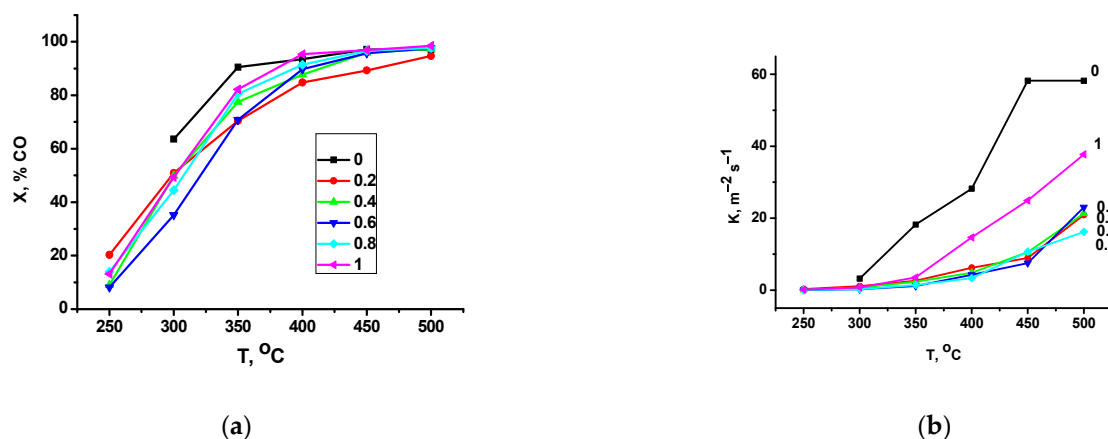


Figure 7. Temperature dependence of CO conversion (a) and CO oxidation rate constant (b) for LaMn_{1-x}Fe_xO₃ perovskites.

It should be noted that in CO oxidation, the catalytic activity of samples measured at 350 °C does not change after their testing at 500 °C. The data obtained indicate that the normalized catalytic activity of LaMn_{1-x}Fe_xO₃ is affected not only by the composition of catalysts and their preparation method, but also by the reaction medium.

Presumably, the higher content of lanthanum on the surface and the depletion with 3d cations lead not only to a lower activity in oxidation reactions of the mixed iron-containing catalysts prepared by the Pechini method, but also to their deactivation at a high content of lanthanum (samples with $x = 0.6$ and 0.8), which is related to the ability of lanthanum oxide to form carbonates and to carbonize. It cannot be ruled out that the activity is also affected by the structurally ordered regions, which are formed under the action of the methane-containing reaction medium on the surface of perovskites, as was noted for the samples with a high substitution degree. The conclusion on the effect exerted by surface enrichment with lanthanum on the activity of catalysts synthesized by the Pechini method agrees with the conclusion made in [10] on a lower activity of the samples obtained by precipitation and containing lanthanum compounds on the surface. Taking into account the dependence between amounts of organics used in the synthesis and content of carbonates on the surface of oxides, which was revealed in [21], by analogy it is expected that the content of carbonates in the oxides prepared by the Pechini method will be higher than in those prepared by the citrate method. It seems that the higher content of lanthanum and hence of carbonates in the samples prepared by the Pechini method changed the form of dependence of activity of the samples on the composition in oxidation reactions because carbonates can block the active sites.

Taking into account the additional effect of reaction inhibition by surface carbonates on the activity, which is more pronounced for compositions with $x = 0.6$ and 0.8 having the highest lanthanum content on the surface, it can be stated that data on the activity in oxidation reactions correlate with TPR data on the amount of adsorbed hydrogen in the first reduction peak. A decrease in adsorption in the first peak with raising the iron content, which testifies to a decrease in the amount of reactive oxygen, correlates with a decrease

in the activity of catalysts in oxidation reactions. An additional effect is exerted by the inhibition by the reaction product, which is more pronounced for compositions with $x = 0.6$ and 0.8 owing to a higher content of lanthanum on the surface. This leads to the observed deviation from the linear dependence between the activity and amount of reactive oxygen.

Thus, the observed changes in the normalized catalytic activity of samples in methane and CO oxidation reactions in dependence on the composition are caused not only by the composition but also by the synthesis method that provided the surface enrichment with lanthanum, which eliminated the dependence between activity and amount of weakly bound oxygen. In a more reducing methane-containing reaction medium, an additional effect on the activity can also be exerted by the ordering of cations. Supposedly, for the reactions that proceed with the involvement of the catalyst oxygen but without inhibition by the reaction product, changes in the activity will correspond to changes in the defect structure of oxides, which determines the content of weakly bound oxygen species.

In this connection, of interest is the high-temperature decomposition of nitrous oxide because this process is determined by oxygen desorption from the surface [22,23]. Figure 8 displays data on the nitrous oxide conversion and reaction rate constants for the tested samples versus temperature. A higher conversion is observed for the mixed oxides with $x = 0.4, 0.6$ and 0.8 , which have a higher specific surface area, whereas the extreme terms of the series have the lowest activity. An estimation of the activity normalized to the unit surface showed that the maximum activity is exhibited by the sample with $x = 0.2$ (Figure 8b). Indeed, data on the activity correlate well with the hydrogen adsorption in the first reduction peak in the region of compositions with $x = 0.2$ – 1 . It means that the modification of lanthanum ferrite with manganese cations, which increases the content of weakly bound oxygen, also increases the activity of catalysts. However, the lanthanum manganite sample, which has the highest amount of weakly bound oxygen but a low activity, falls out of this dependence. The activity of lanthanum manganite in this series is lower than the value expected according to TPR; as shown in [24], this may be caused by a change in the rate-determining stage of the oxygen desorption process, which includes stages of oxygen atoms recombination leading to the formation of oxygen molecules, and the stage of molecular oxygen desorption. If for lanthanum ferrite the rate-determining stage of the oxygen desorption process is exactly the desorption stage (the formation of oxygen molecule does not limit), then for lanthanum manganite it is the stage of oxygen molecule formation. Our earlier study showed that the substitution of lanthanum in lanthanum manganite by strontium also increases the nitrous oxide conversion due to the acceleration of the rate-determining stage—the formation of oxygen molecules. The introduction of iron cations in lanthanum manganite, which also leads to the formation of vacancies, increases the formation rate of oxygen molecules and probably changes the rate-determining stage of the process at $x = 0.2$.

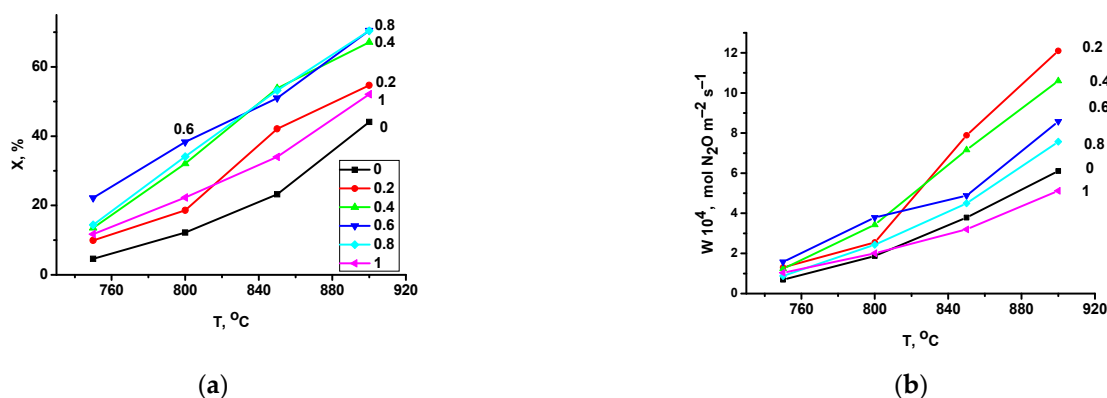


Figure 8. Temperature dependence of nitrous oxide decomposition degree (a) and nitrous oxide decomposition rate (b) for LaMn_{1-x}Fe_xO₃ perovskites.

Thus, in the high-temperature decomposition of nitrous oxide in the absence of inhibition by reaction products, the activity of samples correlates with the degree of substitution, which determines the amount of weakly bound oxygen in the series of compositions with $x = 0.2$ – 1 . Lanthanum manganite ($x = 0$) falls out of this correlation most probably due to the change of the rate-determining stage of nitrous oxide decomposition for this perovskite. The data obtained also demonstrate that activity of the substituted perovskites in N_2O decomposition becomes comparable with the activity of the most active $LaCoO_3$ perovskite [3].

3. Materials and Methods

3.1. Preparation of the Catalysts

The synthesis of $LaMn_{1-x}Fe_xO_3$ samples with a step of $x = 0.2$ was carried out by the Pechini method and included the dissolution of crystalline hydrates of the corresponding nitrate salts in water, the mixing of the solutions in a desired cationic ratio, and the addition of citric acid and ethylene glycol with the subsequent evaporation at 70 – 80 °C to obtain a rubber-like polymer (a polymer-salt composition). After oxidative destruction of the polymer at 110 °C, the formed precursors were calcined at 900 °C for 4 h.

3.2. Characterization of the Catalysts

X-ray diffraction patterns of the samples were obtained on an HZG 4-C (Freiberger Präzisionsmechanik, Freiberg, Germany) diffractometer using monochromatic (a flat diffracted-beam graphite monochromator) CuK_{α} radiation in the angular range of 10 – 75° (2θ) and point-by-point scanning. A scanning step was 0.05° , and the accumulation time in each point was 3 s. Unit cell parameters were calculated using the Polycrystal software package [25]. CSR parameters and $\Delta d/d$ micro-distortions were calculated according to the Selyakov-Scherrer equation in a cubic unit cell approximation using the formula $\beta \cos \theta = \lambda/D + 4(\Delta d/d) \sin \theta$.

High resolution transmission electron microscopy (HRTEM) data were obtained on a JEM-2010 (JEOL, Tokyo, Japan) instrument with a resolution of 1.4 Å. Energy dispersive X-ray analysis (EDX) of the elemental composition of samples was performed on an EDX spectrometer with an Si(Li) detector having an energy resolution of 130 eV. Prior to the study, particles of the samples were deposited on the perforated carbon substrates fixed on copper or molybdenum grids using a UZD-1UCh2 ultrasonic disperser to obtain a uniform distribution of the particles over the substrate surface.

The chemical composition of the catalyst surface was examined using a SPECS Surface Nano Analysis GmbH (Berlin, Germany) photoelectron spectrometer equipped with a hemispherical analyzer PHOIBOS-150-MCD-9, X-ray monochromator FOCUS-500, and an XR-50M source of characteristics radiation with a double Al/Ag anode. The spectra were recorded using a monochromatic Al K_{α} source ($h\nu = 1486.74$ eV).

The specific surface area was determined by the BET method from the thermal desorption of argon.

The temperature-programmed reduction with hydrogen (H_2 -TPR) was performed in a flow setup with a thermal conductivity detector to examine the catalyst samples with the grain size of 0.25 – 0.50 mm. The samples were pretreated in oxygen at 500 °C for 30 min and then cooled in oxygen to room temperature. The weight of the sample was 50 mg; and the reducing medium (10% H_2 in argon) was fed at a rate of 40 mL/min. The samples were heated to 900 °C at a rate of 10° /min. The amount of adsorbed hydrogen was calculated using the Origin software package over the temperature regions of 40 – 550 and 40 – 900 °C.

3.3. Catalytic Tests

The catalytic activity toward the oxidation of methane was estimated for the catalysts with 0.25 – 0.5 mm grain size at 350 – 600 °C in a flow-type setup equipped with a chromatographic analysis unit. Prior to each measurement, the sample was held in the reaction medium (0.9% CH_4 + 9% O_2 + 90.1% N_2 , flow rate 2.4 L/h, and contact time 1.5 s) for

ca. 30 min. The products of methane oxidation were carbon dioxide and water only. The reaction rate was calculated under the assumption of its plug-flow mode using the formula:

$$w = 2.69 \times 10^{19} k C_0 (\text{CH}_4 \text{ molecules}) \text{ m}^{-2} \text{ s}^{-1} \quad (1)$$

where k is the reaction rate constant, $k = -\ln(1 - x)/\tau S_{\text{sp}} \text{ m, m}^{-2} \text{ s}^{-1}$ (x —the methane conversion; τ —the contact time, s; m —the sample weight, g; S_{sp} —the specific surface area of the sample, m^2/g), and C_0 is the initial concentration of methane (%). After testing at 300, 350, 400, 450, 500 and 550 °C, the sample was cooled to 350 °C in the reaction mixture flow, and its activity was estimated once more.

The catalytic activity in CO oxidation was measured in a flow-circulation setup using the catalyst fraction with the grain size of 0.25–0.5 mm. A mixture of 1 g catalyst and 1 cm^3 quartz was loaded in a tubular quartz reactor with the diameter of 15 mm. The reaction mixture 1% CO + 1% O₂ (N₂ the balance) was fed at a rate of 10 L/h; the circulation rate was 1000 L/h. Before the experiment, the sample was held in a flow of artificial air with the composition 20% O₂ + 80% N₂ (5 L/h) at 400 °C for 1 h and then cooled. Prior to each measurement, the sample was held in the reaction mixture at a specified temperature for 30 min. The rate constant was calculated under the assumption of perfect mixing mode of the reaction using the formula:

$$k = X_{\text{CO}} / [(1 - X_{\text{CO}}) \cdot N \cdot S_{\text{sp}} \cdot \tau] \text{ m}^{-2} \text{ s}^{-1} \quad (2)$$

where X_{CO} is the CO conversion; N —the catalyst weight, g; S_{sp} —the specific surface area, m^2/g ; and τ —the contact time, s. After testing at 300, 350, 400, 450 and 500 °C, the sample was cooled in the reaction medium flow to 350 °C, and its activity was measured once more.

The catalytic activity in nitrous oxide decomposition was estimated at 750–900 °C in a flow setup equipped with a chromatographic analysis unit. 10 mg samples of the catalyst with the grain size 0.25–0.5 mm were used. Contact time was 0.001 s at a 1 L/min consumption of the reaction mixture with the composition 0.15% N₂O + 3% O₂ + 3% H₂O (He the balance). A preliminary experiment excluded the effect of external diffusion limitations and the occurrence of homogeneous reaction in an empty reactor.

The catalytic activity was classified by the first order reaction rate W of N₂O decomposition according to the following equations:

Reaction rate at the reactor inlet, $\text{mol N}_2\text{O}/\text{m}^2 \times \text{s}$

$$W = k C_0 / S q \quad (3)$$

First order reaction rate constant, 1/s

$$k = \tau^{-1} \ln C_0 / C \quad (4)$$

Residence time (contact time), s

$$\tau = 17,880 v P / (273 + T) V \quad (5)$$

where C_0 and C are concentrations of N₂O in the inlet and outlet mixtures (mol), respectively; V —the total flow rate (ml/min), T —the reaction temperature (°C), P —the pressure in the reactor (atm); v —the catalyst volume (ml), q —the catalyst weight (g); and S —the BET surface area (m^2/g).

4. Conclusions

- Perovskite samples of the $\text{LaMn}_{1-x}\text{Fe}_x\text{O}_3$ ($x = 0-1$) series were prepared by the Pechini method; their physicochemical properties were studied and catalytic activity was estimated in methane and CO oxidation and nitrous oxide decomposition reactions.
- Samples with the composition $x < 0.4$ were shown to be the orthorhombic perovskites, whereas samples with $x > 0.4$ were the rhombohedral ones. Both modifications are

present in the sample with $x = 0.4$, which indicates that the morphotropic phase transition occurs in the systems in the composition region with $x \sim 0.4$. The TPR study revealed that an increase in the x value decreases the amount of weakly bound oxygen and lowers the temperature at which the reduction starts. Specific surface area values change through the maxima at $x = 0.8$. The XPS study demonstrated that the surface of the samples with $0 < x < 1$ prepared by the Pechini method is enriched with lanthanum compounds.

- All of the intermediate samples of the series were shown to have a lower normalized per m^2 catalytic activity in CO and methane oxidation reactions as compared to extreme terms of the series; therefore, LaMnO_3 was more active than LaFeO_3 . The observed dependence of the samples' activity with an increase in the x value cannot be attributed only to a decrease in the content of weakly bound oxygen species, which behave in a linear manner with an increase in x . An additional effect is exerted by an increase in the content of lanthanum compounds on the surface, which leads to blocking of the surface by the reaction product (CO_2) that forms surface carbonates with lanthanum compounds. The higher the content of lanthanum on the surface, the more pronounced is the detected decrease in activity. It cannot be ruled out also that an additional decrease in activity of the samples with high iron content during methane oxidation is promoted by the formation of locally ordered regions and carbon on the surface of these oxides upon testing. So, the best normalized per m^2 activity in methane and CO oxidation among the studied perovskites was revealed for LaMnO_3 .
- It was shown that all of the intermediate samples of the series, on the contrary, are more active in the high-temperature decomposition of nitrous oxide than the extreme terms of the series; the maximum normalized catalytic activity was observed for the sample with $x = 0.2$. A decrease in activity with the growth of x in the series with $x = 0.2\text{--}1$ correlates with the content of weakly bound oxygen species in the samples. Lanthanum manganite may fall out of the correlation due to the difference in the rate-determining stage of the process in the case of this oxide. Therefore, the best normalized per m^2 activity in high-temperature N_2O decomposition was revealed for $\text{LaMn}_{0.2}\text{Fe}_{0.8}\text{O}_3$.
- Different dependences of activities on the catalyst's composition or amount of weakly bound oxygen species in the samples obtained in the study for the tested reactions, which are implemented with participation of the catalyst oxygen, are caused by the effect of characteristic features of the reaction mechanisms and the preparation method.

Author Contributions: L.I.—methodology, conceptualization, supervision; V.R.—investigations; E.G.—investigations; I.P.—investigations. All authors have read and agreed to the published version of the manuscript.

Funding: This work was supported by the Ministry of Science and Higher Education of the Russian Federation within the governmental order for Boreskov Institute of Catalysis, project AAAA-A21-121011490008-3.

Data Availability Statement: Informed consent was obtained from all subjects involved in the study.

Conflicts of Interest: The authors declare that they have no conflict of interest.

References

1. Zhang, W.; Tang, Y.; Yin, Y.; Gong, W.; Song, J.; Ma, Y.; Ruan, M.; Xu, H.; Chen, D. Research progress in enhanced catalytic oxidation of VOCs by modified La-based perovskite catalyst. *Chem. Ind. Eng. Progress* **2021**, *40*, 1425–1437.
2. Huang, H.F.; Sun, Z.; Lu, H.F.; Shen, L.Q.; Chen, B.V.; Ust, Y. Perovskite catalysts for methane combustion: Applications, design, effects for reactivity and partial oxidation. *Energy Res.* **2019**, *43*, 7755–7789.
3. Russo, N.; Mescia, D.; Fino, D.; Saracco, G.; Specchia, V. N_2O decomposition over perovskite catalysts. *Ind. Eng. Chem. Res.* **2007**, *46*, 4226–4231. [[CrossRef](#)]
4. Labhasetwar, N.; Saravanan, G.; Megarajan, S.K.; Manwar, N.; Khobragade, R.; Doggali, P.; Grasset, F. Perovskite-type catalytic materials for environmental applications. *Sci. Technol. Adv. Mater.* **2015**, *16*, 036002. [[CrossRef](#)]

5. Sadykov, V.A.; Isupova, L.A.; Zolotarskii, I.A.; Bobrova, L.N.; Noskov, A.S.; Parmon, V.N.; Brushtein, E.A.; Telyatnikova, T.V.; Chernyshev, V.I.; Lunin, V.V. Oxide catalysts for ammonia oxidation in nitric acid production: Properties and perspectives. *Appl. Catal. A Gen.* **2000**, *204*, 59–87. [[CrossRef](#)]
6. Wang, X.; Wu, T.; Zachariah, M.R. Doped Perovskites to Evaluate the Relationship between Fuel–Oxidizer Thermite Ignition and Bond Energy, Electronegativity, and Oxygen Vacancy. *J. Phys. Chem. C* **2017**, *121*, 147–152. [[CrossRef](#)]
7. Yakovleva, I.S.; Isupova, L.A.; Rogov, V.A.; Sadykov, V.A. Forms of oxygen in $\text{La}_{1-x}\text{Ca}_x\text{MnO}_{3+\delta}$ ($x = 0-1$) perovskites and their reactivities in oxidation reactions. *Kinet. Catal.* **2008**, *49*, 261–270. [[CrossRef](#)]
8. Miao, F.; Wang, F.; Mao, D.; Guo, X.; Yu, J.; Huang, H.; Lu, G. Effect of different reaction conditions on catalytic activity of $\text{La}(\text{Mn}, \text{Fe})\text{O}_{3+\lambda}$ catalyst for methane combustion. *Mater. Res. Express* **2019**, *6*, 055001. [[CrossRef](#)]
9. Ivanov, D.V.; Pinaeva, L.G.; Sadovskaya, E.M.; Isupova, L.A. Influence of the mobility of oxygen on the reactivity of $\text{La}_{1-x}\text{Sr}_x\text{MnO}_3$ perovskites in methane oxidation. *Kinet. Catal.* **2011**, *52*, 401–408. [[CrossRef](#)]
10. Zheng, S.; Hua, Q.; Gu, W.; Liu, B. Catalytic oxidation of CO on $\text{LaMn}_{1-x}\text{Fe}_x\text{O}_3$ perovskites solid solution. *J. Mol. Catal. A Chem.* **2014**, *391*, 7–11. [[CrossRef](#)]
11. Isupova, L.A.; Tsybulya, S.V.; Kryukova, G.N.; Alikina, G.M.; Boldyreva, N.N.; Yakovleva, I.S.; Ivanov, V.P.; Sadykov, V.A. Real structure and catalytic activity of $\text{La}_{1-x}\text{Ca}_x\text{MnO}_3$ perovskites. *Solid State Ion.* **2001**, *141–142*, 417–425. [[CrossRef](#)]
12. Zhu, J.; Li, H.; Zhong, L.; Xiao, P.; Xu, X.; Yang, X.; Zhao, Z.; Li, J. Perovskite Oxides: Preparation, Characterizations, and Applications in Heterogeneous Catalysis. *ACS Catal.* **2014**, *4*, 2917–2940. [[CrossRef](#)]
13. Wołczyr, M.; Horyn, R.; Bourée, F.; Bukowska, E. Structural defects in LaMnO_3 phase studied by neutron diffraction. *J. Alloys Compd.* **2003**, *353*, 170–174. [[CrossRef](#)]
14. Mizusaki, J.; Sasamoto, T.; Cannon, W.R.; Bowen, H.K. Electronic Conductivity, Seebeck Coefficient, and Defect Structure of LaFeO_3 . *J. Am. Ceram. Soc.* **2006**, *65*, 363–368. [[CrossRef](#)]
15. Tarjomannejad, A.; Farzi, A.; Gómez, M.J.I.; Niaei, A.; Salari, D.; Albaladejo-Fuentes, V. Catalytic Reduction of NO by CO over $\text{LaMn}_{1-x}\text{Fe}_x\text{O}_3$ and $\text{La}_{0.8}\text{A}_{0.2}\text{Mn}_{0.3}\text{Fe}_{0.7}\text{O}_3$ ($A = \text{Sr}, \text{Cs}, \text{Ba}, \text{Ce}$) Perovskite Catalysts. *Catal. Lett.* **2016**, *146*, 2330–2340. [[CrossRef](#)]
16. Magalhaes, F.; Moura, F.C.C.; Ardisson, J.D.; Lago, R.M. $\text{LaMn}_{1-x}\text{Fe}_x\text{O}_3$ and $\text{LaMn}_{0.1-x}\text{Fe}_{0.90}\text{Mo}_x\text{O}_3$ Perovskites: Synthesis, Characterization and Catalytic Activity in H_2O_2 Reactions. *Mater. Res.* **2008**, *11*, 307–312. [[CrossRef](#)]
17. Zheng, J.; Liu, J.; Zhao, Z.; Xu, J.; Jiang, G. The synthesis and catalytic performances of three-dimensionally ordered macroporous perovskite-type $\text{LaMn}_{1-x}\text{Fe}_x\text{O}_3$ complex oxide catalysts with different pore diameters for diesel soot combustion. *Catal. Today* **2012**, *191*, 146–153. [[CrossRef](#)]
18. Zhou, Z.; Pederson, L.R.; Cai, Q.; Jang, J.; Scarfino, B.J.; Kim, M.; Yelon, W.B.; James, W.J.; Anderson, H.U.; Wang, C. Structural and magnetic properties of $\text{LaMn}_{1-x}\text{Fe}_x\text{O}_3$ ($0 < x < 1.0$). *J. Appl. Phys.* **2006**, *99*, 08M918.
19. Isupova, L.A.; Gerasimov, E.Y.; Zaikovskii, V.I.; Tsybulya, S.V. Effect of the Reaction Medium on the Structure of the $\text{La}_{1-x}\text{Ca}_x\text{MnO}_3$ ($x = 0-1$) Solid Solutions Prepared by the Pechini Method. *Kinet. Catal.* **2011**, *52*, 104–110. [[CrossRef](#)]
20. Sedykh, V.; Shekhtman, V.S.; Zverkova, I.I.; Dubovitskii, A.V.; Kulakov, V.I. Reversibility of structure phase transitions in $\text{LaMnO}_{3+\delta}$ manganite under heat treatment. *Phys. C* **2006**, *433*, 189–194. [[CrossRef](#)]
21. Belysheva, D.N.; Sinelshchikova, O.Y.; Tyurnina, N.G.; Tyurnina, Z.G.; Sviridov, S.I.; Tumarkin, A.V.; Zlygostov, M.V.; Ugolkov, V.L. Glycine–Nitrate Synthesis of Solid Solutions of Barium–Strontium Metatitanate. *Phys. Solid State* **2019**, *61*, 2371. [[CrossRef](#)]
22. Mengli, L.; Xiaolong, Y.; Liping, T.; Xumao, X.; Sili, R.; Hu, B.H. Catalysts for Catalytic Decomposition of Nitrous Oxide. *Prog. Chem.* **2012**, *9*, 1801–1817.
23. Konsolakis, M. Recent Advances on Nitrous Oxide (N_2O) Decomposition over Non-Noble-Metal Oxide Catalysts: Catalytic Performance, Mechanistic Considerations, and Surface Chemistry Aspects. *ACS Catal.* **2015**, *5*, 6397–6421. [[CrossRef](#)]
24. Ivanov, D.V.; Pinaeva, L.G.; Sadovskaya, E.M.; Isupova, L.A. Isotopic transient kinetic study of N_2O decomposition on $\text{LaMnO}_{3+\delta}$. *J. Mol. Catal. A Chem.* **2016**, *412*, 34–38. [[CrossRef](#)]
25. Tsybulya, S.V.; Cherepanova, S.V.; Soloviova, L.P. Polycrystal software package for IBM/PC. *J. Struct. Chem.* **1996**, *37*, 332–334. [[CrossRef](#)]